

Novel Coexistence of Superconductivity with Two Distinct Magnetic Orders

A. D. Christianson,^{1,2} A. Llobet,¹ Wei Bao,^{1,*} J. S. Gardner,^{3,4,†} I. P. Swainson,³ J. W. Lynn,⁴ J.-M. Mignot,⁵ K. Prokes,⁶ P. G. Pagliuso,^{1,‡} N. O. Moreno,¹ J. L. Sarrao,¹ J. D. Thompson,¹ and A. H. Lacerda¹

¹Los Alamos National Laboratory, Los Alamos, New Mexico 87545, USA

²Colorado State University, Fort Collins, Colorado 80523, USA

³NRC Canada, NPMR, Chalk River Laboratories, Chalk River, Ontario K0J 1J0, Canada

⁴NIST Center for Neutron Research, National Institute of Standards and Technology, Gaithersburg, Maryland 20899, USA

⁵Laboratoire Léon Brillouin, CEA-CNRS, CEA/Saclay, 91191 Gif-sur-Yvette, France

⁶BENSC, Hahn-Meitner-Institut, Glienickestrass 100, D-14109, Berlin, Germany

(Received 13 July 2005; published 15 November 2005)

The heavy fermion $\text{CeRh}_{1-x}\text{Ir}_x\text{In}_5$ system exhibits properties that range from an incommensurate antiferromagnet for small x to an exotic superconductor on the Ir-rich end of the phase diagram. At intermediate x where antiferromagnetism coexists with superconductivity, two types of magnetic order are observed: the *incommensurate* one of CeRhIn_5 and a new, *commensurate* antiferromagnetism that orders separately. The coexistence of f -electron superconductivity with two distinct f -electron magnetic orders is unique among unconventional superconductors, adding a new variety to the usual coexistence found in magnetic superconductors.

DOI: 10.1103/PhysRevLett.95.217002

PACS numbers: 74.70.Tx, 71.27.+a, 75.20.Hr, 75.25.+z

Magnetism and superconductivity are two major cooperative phenomena in condensed matter, and the relationship between them has been studied extensively. Conventional superconductivity in phonon mediated s -wave materials is susceptible to the Cooper-pair breaking by magnetic scattering [1,2]. In cases where superconductivity and magnetic order coexist, such as rare-earth based molybdenum chalcogenides, rhodium borides, and borocarbides, the superconducting d electrons and localized f electrons are weakly coupled, and the competition between superconductivity and magnetic order is understood [2,3] in terms of the theory of Abrikosov and Gorkov [1]. In contrast, strong magnetic fluctuations have been observed in heavy fermion, cuprate, and ruthenate superconductors [4–7], and magnetic excitations have been proposed to mediate the Cooper pairing in these unconventional superconductors [8–13]. Some of the U-based heavy fermion compounds form an interesting subset of these superconductors where superconductivity develops out of a magnetically ordered state. For UPd_2Al_3 [14,15] the magnetic state is a commensurate antiferromagnet, for UNi_2Al_3 [16,17] an incommensurate antiferromagnet, for UGe_2 [18] and URhGe [19] a ferromagnet. For UPt_3 [20], three distinct superconducting phases [21–23] coexist with a commensurate short-range antiferromagnetic order. In analogy to superfluid ^3He , intriguing coupling between the magnetic and superconducting order parameters has been proposed [8].

Recently a new family of Ce-based heavy fermion materials has been discovered, which sets a record superconducting transition temperature of $T_C = 2.3$ K for heavy fermion materials [24–26]. The coexistence of magnetic order and superconductivity is observed in a wide composition range in $\text{CeRh}_{1-x}\text{Ir}_x\text{In}_5$ [27] [see Fig. 1(a)]; previously superconductivity was found only in heavy

fermion materials of the highest purity [18]. At one end of the $\text{CeRh}_{1-x}\text{Ir}_x\text{In}_5$ series, CeIrIn_5 is a superconductor below $T_C = 0.4$ K [25]. At the other end, CeRhIn_5 orders magnetically below $T_{Ni} = 3.8$ K in an antiferromagnetic

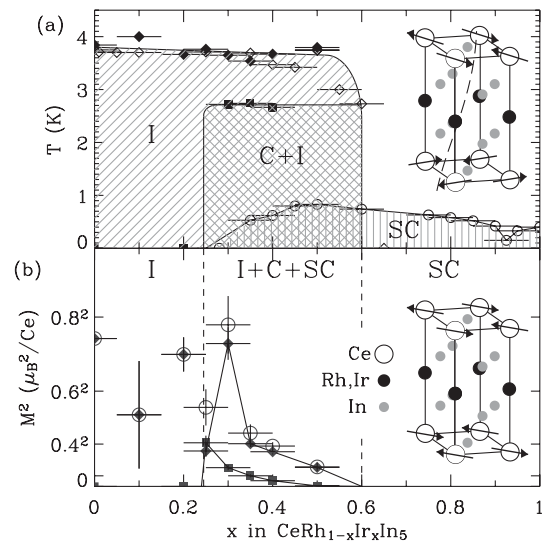


FIG. 1. (a) Temperature-composition phase diagram for $\text{CeRh}_{1-x}\text{Ir}_x\text{In}_5$. There are three distinct long-range orders: superconducting (SC), incommensurate antiferromagnetic (I), and commensurate antiferromagnetic (C). The diamonds represent the Néel temperature for the I phase, squares for the C phase, and circles for T_C of the SC phase. The open symbols are from previous work [27], and the closed symbols from this work. (b) Diamonds and squares represent squared magnetic moments at 1.9 K for the I and C phases, respectively. The circles represent the square of the total magnetic moment per Ce in Eq. (4). The solid lines are guides to the eye. The dashed lines delimit the I, I + C + SC, and SC phases. Magnetic structures of the I and C phases are shown as insets to (a) and (b), respectively.

spiral structure with an ordering wave vector $\mathbf{q}_i = (\frac{1}{2}, \frac{1}{2}, \pm\delta)$, $\delta = 0.297$ [28], that is incommensurate with the tetragonal crystal lattice [29]. In the overlapping region of superconducting and antiferromagnetic phases, $0.25 \leq x \leq 0.6$, we find unexpectedly an additional commensurate antiferromagnetic order that develops separately below $T_{Nc} = 2.7$ K. This makes Ce(Rh, Ir)In₅ unique among unconventional superconductors in that the ground state exhibits the coexistence of the superconducting order parameter with two distinct magnetic order parameters.

Single crystals of CeRh_{1-x}Ir_xIn₅ were grown from an In flux with appropriate ratio of Rh and Ir starting materials [27]. Lattice parameters follow Vegard's law and the sample composition x is estimated to be within ± 0.05 of the nominal composition [27]. Samples used in this work were cut to a thickness ~ 1.3 mm to minimize problems due to the high neutron absorption of Rh, Ir, and In. The search for and collection of magnetic Bragg neutron diffraction peaks in CeRh_{1-x}Ir_xIn₅ ($x = 0.1, 0.2, 0.25, 0.3, 0.35, 0.4, \text{ and } 0.5$) were performed at the thermal triple-axis spectrometers C5 and N5 of Chalk River Laboratories, and BT2 and BT7 of NIST. Neutrons with incident energy $E_i = 35$ meV were selected using the (113) reflection of a Ge crystal, the (002) of a Be crystal, or the (002) of a pyrolytic graphite monochromator. At this energy, the neutron penetration length is longer than the sample thickness. Polarized neutron diffraction experiments were performed at BT2 of NIST with $E_i = 14.7$ meV on a $x = 0.3$ sample to verify magnetic signals and to determine magnetic moment orientation. Pyrolytic graphite filters were employed when appropriate to remove higher order neutrons. The sample temperature was controlled by a top-loading pumped ⁴He cryostat at both Chalk River and NIST. Additional measurements of magnetic order parameters were performed at the triple-axis spectrometer 4F2 of LLB-Saclay using a pumped ⁴He cryostat, and at the E4 diffractometer of BENSCL using a dilution refrigerator.

In a previous heat capacity study [27], a phase transition was observed in the range of 3.8 to 2.7 K for $0 \leq x \leq 0.6$, and was attributed to an antiferromagnetic transition as in CeRhIn₅ [24] [open diamonds in Fig. 1(a)]. This is confirmed by the results of this neutron diffraction work which show that all samples ($0.1 \leq x \leq 0.5$) have magnetic Bragg peaks characterized by the same incommensurate wave vector as in CeRhIn₅ [28]. The Néel temperature, T_{Ni} , determined from the temperature variation of magnetic Bragg peaks is shown as filled diamonds in Fig. 1(a).

Thermodynamic and transport measurements uncover a superconducting state below 1 K in a wide composition range, $0.25 \leq x \leq 1$ [27] [open circles in Fig. 1(a)]. In $0.25 \leq x \leq 0.6$ where the superconducting and incommensurate antiferromagnetic phases coexist, we find a second magnetic order below 2.7 K with a commensurate antiferromagnetic ordering wave vector $\mathbf{q}_c = (\frac{1}{2}, \frac{1}{2}, \frac{1}{2})$ [filled squares in Fig. 1].

Table I lists integrated intensities of magnetic Bragg peaks at 1.9 K for $x = 0.3$ of both commensurate and incommensurate types, collected by rocking scans in the two-axis mode and normalized to structural Bragg peaks (002), (003), (004), (006), (111), (112), (113), (220), (221), and (222) to yield magnetic neutron diffraction cross sections in absolute units, $\sigma(\mathbf{q}) = I(\mathbf{q}) \sin(2\theta)$, where 2θ is the scattering angle. In such units, the magnetic cross section is [30]

$$\sigma(\mathbf{q}) = \left(\frac{\gamma r_0}{2}\right)^2 M_{i,c}^2 |f(q)|^2 \sum_{\mu,\nu} (\delta_{\mu\nu} - \hat{\mathbf{q}}_\mu \hat{\mathbf{q}}_\nu) \mathcal{F}_\mu^*(\mathbf{q}) \mathcal{F}_\nu(\mathbf{q}), \quad (1)$$

where $(\gamma r_0/2)^2 = 0.07265$ barns/ μ_B^2 , $M_{i,c}$ is the staggered moment of the Ce ion in either the incommensurate or commensurate antiferromagnetic structure, $f(q)$ the magnetic form factor which could be different for the two type antiferromagnetic orders, $\hat{\mathbf{q}}$ the unit vector of \mathbf{q} , and $\mathcal{F}_\mu(\mathbf{q})$ the μ th Cartesian component of the magnetic structure factor per molecular formula.

The incommensurate magnetic structure for CeRhIn₅ has been determined [inset in Fig. 1(a)] and the magnetic cross section, Eq. (1), is reduced to [28]

$$\sigma^i(\mathbf{q}) = \frac{1}{4} \left(\frac{\gamma r_0}{2}\right)^2 M_i^2 |f(q)|^2 (1 + |\hat{\mathbf{q}} \cdot \hat{\mathbf{c}}|^2), \quad (2)$$

where $\hat{\mathbf{c}}$ is the unit vector of the c axis.

For the commensurate magnetic component, the summation in Eq. (1) is reduced to $(1 - |\hat{\mathbf{q}} \cdot \hat{\mathbf{M}}_c|^2) |\mathcal{F}(\mathbf{q})|^2$, where $\hat{\mathbf{M}}_c$ is the unit vector of the magnetic moment, and $|\mathcal{F}(\mathbf{q})|^2 = 1$. Polarized neutron diffraction measurements

TABLE I. Magnetic Bragg intensity, σ_{obs} , defined in Eq. (1), observed at 1.9 K in units of 10^{-3} barns per CeRh_{0.7}Ir_{0.3}In₅. The theoretical intensity, σ_{cal} , is calculated using Eqs. (2) and (3) for the incommensurate moment $M_i = 0.73 \mu_B/\text{Ce}$ and the commensurate moment $M_c = 0.27 \mu_B/\text{Ce}$, respectively.

\mathbf{q}	σ_{obs}	σ_{cal}	\mathbf{q}	σ_{obs}	σ_{cal}
$(\frac{1}{2}, \frac{1}{2}, \delta)$	9.0(5)	9.3	$(\frac{1}{2}, \frac{1}{2}, 1 - \delta)$	10.1(3)	10.8
$(\frac{1}{2}, \frac{1}{2}, 1 + \delta)$	9.6(3)	12.1	$(\frac{1}{2}, \frac{1}{2}, 2 - \delta)$	9.9(3)	12.0
$(\frac{1}{2}, \frac{1}{2}, 2 + \delta)$	9.0(3)	10.8	$(\frac{1}{2}, \frac{1}{2}, 3 - \delta)$	8.2(4)	9.6
$(\frac{1}{2}, \frac{1}{2}, 3 + \delta)$	5.7(3)	7.7	$(\frac{1}{2}, \frac{1}{2}, 4 - \delta)$	5.7(3)	6.5
$(\frac{1}{2}, \frac{1}{2}, 4 + \delta)$	4.3(3)	4.9	$(\frac{1}{2}, \frac{1}{2}, 5 - \delta)$	3.9(3)	3.9
$(\frac{1}{2}, \frac{1}{2}, 5 + \delta)$	2.9(3)	2.7	$(\frac{1}{2}, \frac{1}{2}, 6 - \delta)$	2.7(5)	2.1
$(\frac{3}{2}, \frac{3}{2}, \delta)$	4.3(3)	4.2	$(\frac{3}{2}, \frac{3}{2}, 1 - \delta)$	3.8(4)	4.2
$(\frac{3}{2}, \frac{3}{2}, 1 + \delta)$	5.4(15)	4.2	$(\frac{3}{2}, \frac{3}{2}, 2 - \delta)$	5.0(4)	4.1
$(\frac{3}{2}, \frac{3}{2}, 2 + \delta)$	3.4(3)	3.9	$(\frac{3}{2}, \frac{3}{2}, 3 - \delta)$	2.9(3)	3.6
$(\frac{3}{2}, \frac{3}{2}, 3 + \delta)$	2.5(4)	3.1	$(\frac{1}{2}, \frac{1}{2}, \frac{1}{2})$	2.3(2)	2.6
$(\frac{1}{2}, \frac{1}{2}, \frac{3}{2})$	2.3(4)	3.2	$(\frac{1}{2}, \frac{1}{2}, \frac{5}{2})$	1.9(7)	2.7
$(\frac{1}{2}, \frac{1}{2}, \frac{9}{2})$	0.8(2)	1.1	$(\frac{3}{2}, \frac{3}{2}, \frac{1}{2})$	1.3(2)	1.1
$(\frac{3}{2}, \frac{3}{2}, \frac{3}{2})$	1.2(2)	1.1	$(\frac{3}{2}, \frac{3}{2}, \frac{5}{2})$	0.7(2)	1.0

at $(\frac{1}{2}, \frac{1}{2}, \frac{1}{2})$ and $(\frac{1}{2}, \frac{1}{2}, \delta)$, with a horizontal and vertical magnetic guide field, respectively, indicate that the magnetic moment in the commensurate antiferromagnetic order, like in the incommensurate order [28], lies in the tetragonal basal plane. The commensurate magnetic structure is depicted in the inset in Fig. 1(b). There are in general 8 symmetry-related $\hat{\mathbf{M}}_c$ domains in the sample and the easy axis within the basal plane cannot be determined in a multidomain sample due to the tetragonal symmetry. Assuming equal populations among these domains during our unpolarized neutron diffraction experiment, the magnetic polarization factor averages to [31] $\langle 1 - |\hat{\mathbf{q}} \cdot \hat{\mathbf{M}}_c|^2 \rangle = (1 + |\hat{\mathbf{q}} \cdot \hat{\mathbf{c}}|^2)/2$. Therefore, the magnetic cross section for the commensurate antiferromagnetic order is

$$\sigma^c(\mathbf{q}) = \frac{1}{2} \left(\frac{\gamma r_0}{2} \right)^2 M_c^2 |f(q)|^2 (1 + |\hat{\mathbf{q}} \cdot \hat{\mathbf{c}}|^2). \quad (3)$$

Applying Eqs. (2) and (3) to the data in Table I, a least-square fit yields staggered magnetic moments $M_i = 0.73 \pm 0.25 \mu_B$ and $M_c = 0.27 \pm 0.10 \mu_B$ per $\text{CeRh}_{0.7}\text{Ir}_{0.3}\text{In}_5$ at 1.9 K.

Measured magnetic intensities for $\text{CeRh}_{0.7}\text{Ir}_{0.3}\text{In}_5$ in Table I are plotted in Fig. 2 as a function of $|\mathbf{q}|$ in scaled quantities $4\sigma^i(\mathbf{q})/[(\gamma r_0/2)^2 M_i^2 (1 + |\hat{\mathbf{q}} \cdot \hat{\mathbf{c}}|^2)]$ and $2\sigma^c(\mathbf{q})/[(\gamma r_0/2)^2 M_c^2 (1 + |\hat{\mathbf{q}} \cdot \hat{\mathbf{c}}|^2)]$, which equal the squared magnetic form factor, $|f(q)|^2$ [Eqs. (2) and (3)]. The solid line is $|f(q)|^2$ for Ce^{3+} ion [32]. The fact that the measured data for both commensurate (squares) and incommensurate (diamonds) orders are well described by the solid curve indicates not only the correctness of our magnetic models in Eqs. (2) and (3) for $\text{CeRh}_{0.7}\text{Ir}_{0.3}\text{In}_5$, but also that the Ce^{3+} ($4f^1$) ions are responsible for both commensurate and incommensurate antiferromagnetic orders. This is consistent with the thermodynamic study [27] where entropy reaches the same value at ~ 6 K for all samples from $x = 0$ to $x = 1$, suggesting that the same f electrons

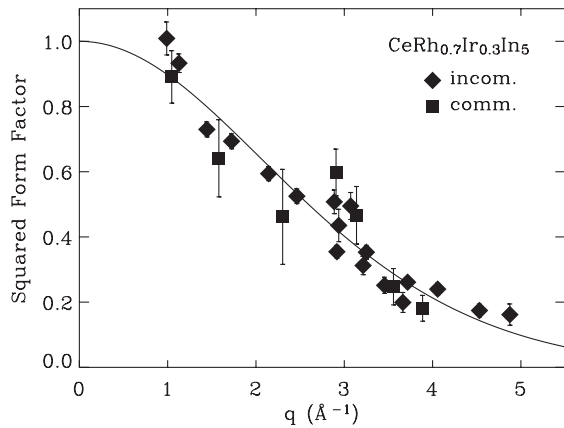


FIG. 2. Both the commensurate (squares) and incommensurate (diamonds) magnetic Bragg peaks follow the magnetic form factor of Ce^{3+} ($4f^1$) ion.

are responsible for heavy fermion formation, antiferromagnetic orders, and superconductivity in $\text{CeRh}_{1-x}\text{Ir}_x\text{In}_5$. Division of the f spectral weight was probed using neutron scattering in CeRhIn_5 [33] and was further investigated in terms of a two-fluid model for this family of heavy fermion materials [34–36].

Magnetic moments for other compositions were measured in a similar fashion, and are shown as squares and diamonds for commensurate and incommensurate structures, respectively, in Fig. 1(b). The average of the squared total magnetic moments per Ce,

$$M^2 \equiv \langle (\mathbf{M}_i + \mathbf{M}_c)^2 \rangle = M_i^2 + M_c^2, \quad (4)$$

is also shown in Fig. 1(b) as circles. A large staggered magnetic moment of $0.85 \mu_B/\text{U}$ [15] coexisting with superconductivity in UPd_2Al_3 has been considered a puzzling anomaly [8], while UPt_3 [20] has a tiny moment of $0.02 \mu_B/\text{U}$, and the moment in UNi_2Al_3 , $0.24 \mu_B/\text{U}$ [17], is also quite small. Here in the coexistence composition region of $\text{Ce}(\text{Rh}, \text{Ir})\text{In}_5$, M ranges from 0.27 to $0.78 \mu_B/\text{Ce}$, bridging the gap between UNi_2Al_3 and UPd_2Al_3 .

In Fig. 3, the temperature dependences of the Bragg peak intensities of $(\frac{1}{2}, \frac{1}{2}, 1 - \delta)$ and $(\frac{1}{2}, \frac{1}{2}, \frac{1}{2})$ are presented as the squared order parameters M_i^2 and M_c^2 of the incommensurate and commensurate antiferromagnetic transitions, respectively. Data below 1.2 K were taken at BENSIC using a dilution refrigerator. There is no thermal hysteresis for either magnetic phase transition. When the commensurate phase transition occurs at 2.7 K, there is no abrupt change in the incommensurate order parameter. Similarly, at the superconducting transition $T_C \approx 0.5$ K (dotted line), no apparent anomaly occurs in either magnetic order parameter. This is analogous to the magnetic order parameter for the heavy fermion superconductors UPd_2Al_3 [37] and UPt_3 in the A and C phases, but different from that for UPt_3 in the superconducting B phase [8,20].

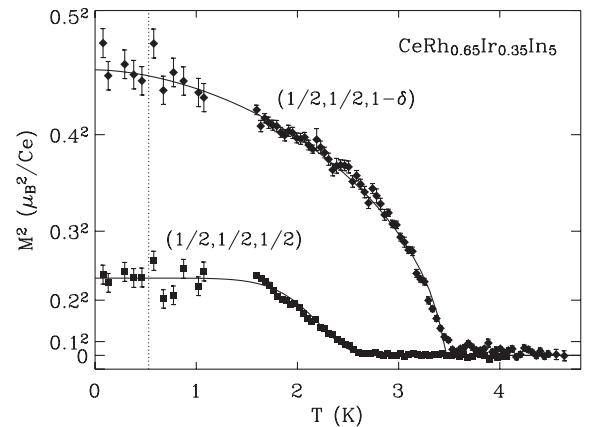


FIG. 3. Squared magnetic order parameters of the incommensurate (diamonds) and commensurate (squares) antiferromagnetic transitions. The dotted line indicates the critical temperature $T_C \approx 0.5$ K of the superconducting transition. The solid lines are guides to the eye.

Note in Fig. 1(a) that the Néel temperatures T_{Ni} and T_{Nc} both are nearly constant when they are nonzero. This might suggest a phase separation scenario where only a volume fraction of $M^2(x)/M^2(0)$ is magnetically ordered and the remaining is superconducting. However, at $x = 0.5$, this would imply $M^2(x)/M^2(0) = 0.08$, which is not consistent with a magnetic volume fraction of at least 0.85 determined from a μ SR study [38].

At the quantum critical point (QCP) of the superconducting phase near $x = 0.25$, the commensurate antiferromagnetic order appears with M_c jumping from zero [Fig. 1(b)]. This suggests a change in electronic structure at $x \approx 0.25$ which produces a strong enough peak at $\mathbf{q} = (\frac{1}{2}, \frac{1}{2}, \frac{1}{2})$ in the RKKY interaction to induce the new magnetic order. Several sheets of the Fermi surface of differently enhanced masses have been observed in the de Haas–van Alphen measurements of CeRhIn₅ and CeIrIn₅ [39,40] and the Fermi surface topology is determined mostly by non- f electrons [41,42]. The concurrence of the superconductivity and commensurate antiferromagnetic order observed here, therefore, suggests that the responsible Fermi surface sheet for the superconductivity may be the one close to nesting at $\mathbf{q} = (\frac{1}{2}, \frac{1}{2}, \frac{1}{2})$.

Both M_i and M_c approach zero at a second QCP of the antiferromagnetism near $x \approx 0.6$, while the Néel temperatures are insensitive to x (Fig. 1). This behavior is similar to UPt₃ under pressure [43], suggesting that both belong to a distinct type of QCP. Recall that $T_N \propto J_{\text{RKKY}} M^2$, where both the RKKY interaction J_{RKKY} and the saturated magnetic moment M are controlled by the Kondo interaction. In both of these systems the divergence of J_{RKKY} and the reduction of M appear to obey $J_{\text{RKKY}} \propto M^{-2}$ as this QCP is approached. Theoretical investigation of the physical process maintaining the delicate proportional relation near this type of QCP is warranted.

In summary, the antiferromagnetic phase of Ce(Rh, Ir)In₅ below ~ 3.8 K is characterized by the incommensurate antiferromagnetic spiral of wave vector $(\frac{1}{2}, \frac{1}{2}, \pm \delta)$. In the coexistence composition region of superconductivity and antiferromagnetism, an additional phase transition to a commensurate antiferromagnet characterized by $(\frac{1}{2}, \frac{1}{2}, \frac{1}{2})$ is discovered below 2.7 K. The same f electron at each site, hybridizing with other conduction electrons, is responsible for both the superconductivity and the commensurate and incommensurate antiferromagnetic orders. It is likely that the energy band(s) with Fermi surface nesting near the $(\frac{1}{2}, \frac{1}{2}, \frac{1}{2})$ is responsible for the heavy fermion superconductivity. The novel coexistence of three different types of cooperative ordered states adds a new variety to the rich phenomena relating to the interplay between magnetism and superconductivity.

We would like to thank G. D. Morris, R. H. Heffner, C. M. Varma, Q. Si, S. A. Trugman, D. Pines, A. Abanov, Y. Bang, P. Dai, and S. Kern for useful discussions, A. Cull for help at CRL, and P. Smeibidl and S.

Gerischer at HMI. Work at Los Alamos was performed under the auspices of the US Department of Energy.

*Electronic address: wbao@lanl.gov

†Current address: Physics Department, Brookhaven National Laboratory, Upton, NY 11973.

‡Current address: Instituto de Física “Gleb Wathagin,” UNICAMP, 13083-970, Campinas, Brasil.

- [1] A. A. Abrikosov and L. P. Gorkov, Zh. Eksp. Teor. Fiz. **39**, 1781 (1960) [Sov. Phys. JETP **12**, 1243 (1961)].
- [2] M. B. Maple, J. Alloys Compd. **303-304**, 1 (2000).
- [3] P. C. Canfield *et al.*, Phys. Today **51**, No. 10, 40 (1998).
- [4] G. Aeppli *et al.*, Phys. Rev. Lett. **58**, 808 (1987).
- [5] M. Braden *et al.*, Phys. Rev. Lett. **88**, 197002 (2002).
- [6] N. Metoki *et al.*, Phys. Rev. Lett. **80**, 5417 (1998).
- [7] N. Bernhoeft *et al.*, Phys. Rev. Lett. **81**, 4244 (1998).
- [8] R. Joynt and L. Taillefer, Rev. Mod. Phys. **74**, 235 (2002).
- [9] K. Miyake *et al.*, Phys. Rev. B **34**, 6554 (1986).
- [10] M. T. Béal-Monod *et al.*, Phys. Rev. B **34**, 7716 (1986).
- [11] J. E. Hirsch, Phys. Rev. Lett. **54**, 1317 (1985).
- [12] P. Monthoux and D. Pines, Phys. Rev. B **47**, 6069 (1993).
- [13] T. M. Rice, Nature (London) **396**, 627 (1998).
- [14] C. Geibel *et al.*, Z. Phys. B **84**, 1 (1991).
- [15] A. Krimmel *et al.*, Z. Phys. B **86**, 161 (1992).
- [16] C. Geibel *et al.*, Z. Phys. B **83**, 305 (1991).
- [17] A. Schröder *et al.*, Phys. Rev. Lett. **72**, 136 (1994).
- [18] S. S. Saxena *et al.*, Nature (London) **406**, 587 (2000).
- [19] D. Aoki *et al.*, Nature (London) **413**, 613 (2001).
- [20] G. Aeppli *et al.*, Phys. Rev. Lett. **63**, 676 (1989).
- [21] G. R. Stewart *et al.*, Phys. Rev. Lett. **52**, 679 (1984).
- [22] R. A. Fisher *et al.*, Phys. Rev. Lett. **62**, 1411 (1989).
- [23] S. Adenwalla *et al.*, Phys. Rev. Lett. **65**, 2298 (1990).
- [24] H. Hegger *et al.*, Phys. Rev. Lett. **84**, 4986 (2000).
- [25] C. Petrovic *et al.*, Europhys. Lett. **53**, 354 (2001); J. Phys. Condens. Matter **13**, L337 (2001).
- [26] M. Nicklas *et al.*, Phys. Rev. B **67**, 020506 (2003).
- [27] P. G. Pagliuso *et al.*, Phys. Rev. B **64**, 100503 (2001).
- [28] W. Bao *et al.*, Phys. Rev. B **62**, R14621 (2000); **67**, 099903(E) (2003).
- [29] E. G. Moshopoulou *et al.*, J. Solid State Chem. **158**, 25 (2001).
- [30] G. L. Squires, *Introduction to the Theory of Thermal Neutron Scattering* (Cambridge University Press, Cambridge, England, 1978).
- [31] W. Bao *et al.*, Phys. Rev. B **64**, 020401(R) (2001).
- [32] M. Blume *et al.*, J. Chem. Phys. **37**, 1245 (1962).
- [33] W. Bao *et al.*, Phys. Rev. B **65**, 100505(R) (2002).
- [34] Y. Bang *et al.*, Phys. Rev. B **66**, 224501 (2002).
- [35] N. J. Curro *et al.*, Phys. Rev. Lett. **90**, 227202 (2003).
- [36] S. Nakatsuji *et al.*, Phys. Rev. Lett. **92**, 016401 (2004).
- [37] B. D. Gaulin *et al.*, Phys. Rev. Lett. **73**, 890 (1994).
- [38] G. D. Morris *et al.*, Physica (Amsterdam) **326B**, 390 (2003).
- [39] Y. Haga *et al.*, Phys. Rev. B **63**, 060503(R) (2001).
- [40] D. Hall *et al.*, Phys. Rev. B **64**, 064506 (2001).
- [41] U. Alver *et al.*, Phys. Rev. B **64**, 180402 (2001).
- [42] J. L. Wang *et al.*, J. Appl. Phys. **93**, 6891 (2003).
- [43] S. M. Hayden *et al.*, Phys. Rev. B **46**, 8675 (1992).